2024 IEEE/RSJ International Conference on Intelligent Robots and Systems (IROS)
October 14-18, 2024. Abu Dhabi, UAE

Automating Trophectoderm Cells Aspiration and Separation in Embryo Biopsy at the Blastocyst Stage: A Vision-Based Control Approach

Ihab Abu Ajamieh Mohammad Al Saaideh Mohammad Al Janaideh James K. Mills

Abstract— **Reproductive medicine has recently witnessed significant advancements, particularly in vitro fertilization (IVF). One crucial aspect of IVF involves the extraction of cellular material and its analysis to maximize the chance of successful implantation. This work highlights the development and application of the automated system for Trophectoderm cell (TE) extraction and separation, addressing the need for precision, efficiency, and reduced manual intervention. The presented automated system is equipped with a computer vision algorithm, microliter pump, vacuum system, and micromanipulation tools to consistently and accurately biopsy TE cells. An experimental setup is developed to verify the behavior of the proposed method, in which a holding micropipette is connected to a vacuum system and holds the embryo stationary. Three steps are performed to complete the process and are controlled by a computer vision algorithm. The coordinates of the Zona Pellucida (ZP) perforation (perforated in a previous step) are used as a feedback signal to a simple proportional controller to control the biopsy pipette motion. The computer vision monitors the amount of TE cells aspirated inside the biopsy pipette and controls the microliter pump. The aspirated TE cells were separated away using a laser cutting system. Experimental results demonstrate that the system can relocate the biopsy pipette, TE cell extraction, and separation.**

I. Introduction

The automation of TE cells extraction is a significant leap in reproductive medicine, offering efficiency and precision to the TE cells biopsy. This automation boosts success rates in assisted reproduction, promising a brighter future for reproductive healthcare [1], [2]. TE cells form the outer layer of the embryo and are paramount in this process. TE cells biopsy and subsequent genetic analysis can provide critical insights into the health and viability of embryos, improving the outcomes of assisted reproductive technologies. Automation technologies offer a high level of precision in TE cells extraction [3]. Robotic systems equipped with imaging algorithms and micromanipulation tools can consistently and accurately biopsy TE cells, reducing the risk of damage to the embryo [4]–[6]. Three main methods are used for the cells' extraction depending on the embryo stage and morphology: Aspiration, embryo squeezing, and fluid flow displacement [7]. The most widely used method is the aspiration method for many reasons: It is easy, simple, extracts the exact targeted cells, and is applicable for all the embryo stages. The European Society of Human Reproduction and Embryology (ESHRE) recommends this method as it is safe for the embryo [8]. The other methods are mainly used for the polar body and blastomere stage, these two methods are not completely guaranteed. In the extrusion method, the ZP is penetrated close to the targeted blastomere, and a pipette with a blunt tip is then used to push the embryo from another side and squeeze it to extrude one or two blastomeres [9], [10]. Due to the complications of this method and the severe stresses applied to the embryo, it is not practiced [11].

In the fluid flow displacement method, the ZP is penetrated in two different positions; one is used as an exit, while the other is used for pumping medium inside the perivitelline space to displace a single blastomere outside the embryo through the exit penetration [12]–[14]. Wong C. and Mills J. used this method to extract a single blastomere from a 4-cell embryo [14]. Their proposed method employs computer-controlled syringe pumps, micromanipulators, and computer vision algorithms. Shan G. *et al*. introduce a robotic biopsy system for cutting and collecting TE cells from a blastocyst [4]. The system employs a convolutional neural network to detect TE cells junctions during laser ablation.

II. Main Contributions

The primary goal of this research is to reduce human-operator involvement through automation, thereby minimizing processing time and variations in repeatability and any other related issues. Additionally, this research seeks to introduce innovative automation techniques for the TE cells aspiration and separation as a step integrated into the whole biopsy procedure at the blastocyst stage and other microsurgery procedures. These techniques are designed for mouse embryos, which closely resemble human embryos in size. These automation methods rely on real-time vision-based feedback control to ensure precision throughout each procedure step as depicted in Figure 1. All the techniques were designed to utilize the conventional tools that are currently in use in any lab or IVF clinics for manual approaches.

III. Experimental setup

In the proposed experimental setup, the embryo is carefully positioned on an inverted microscope (Nikon Ti-U), which is equipped with a high-speed sCMOS camera (QImaging optiMOS) to capture images with a precise exposure time of 9 µs. A microscope objective with 20x magnification is employed to ensure clear and detailed imaging and

Ihab Abu Ajamieh is with Mechanical and Mechatronics Engineering Department, Birzeit University, PO Box 14, Birzeit West Bank, Palestine. iabuajamieh@birzeit.edu. Ihab is the corresponding author.

M. Al Saaideh is with the Department of Mechanical and Mechatronics Engineering, Memorial University, St. John's, Newfoundland A1B 3X5, Canada. mailsaaideh@mun.ca.

M. Al Janaideh is with the School of Engineering, University of Guelph, Guelph, ON N1G 2W1, Canada. maljanai@uoguelph.ca

J. K. Mills is with the Department of Mechanical and Industrial Engineering at the University of Toronto. Toronto, Ontario, M5S 3G8 Canada. mills@mie.utoronto.ca.

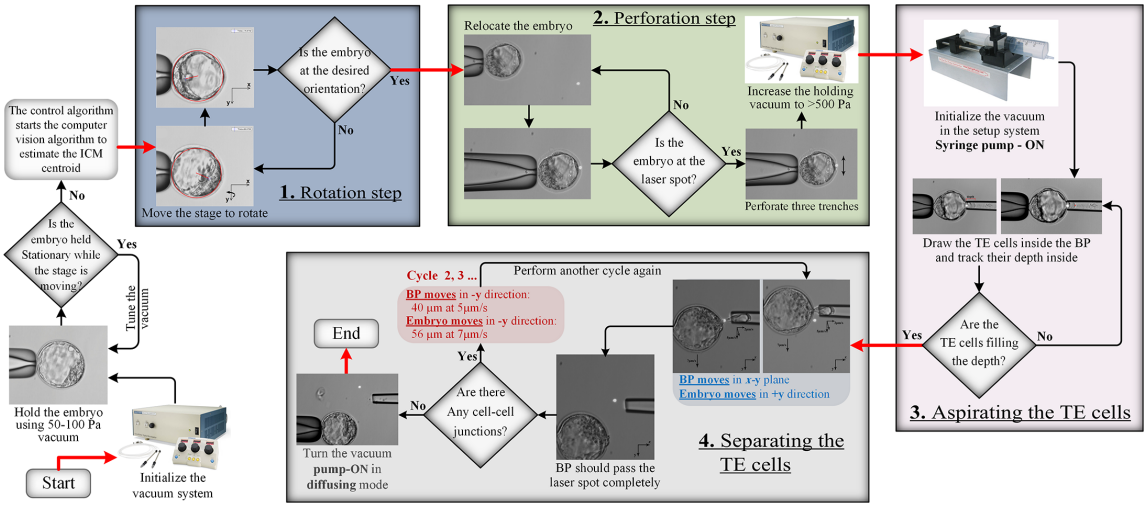

Fig. 1: The steps of the embryo biopsy procedure. (1) The embryo reorientation. (2) The embryo perforation. (3) Aspirating the TE cells. (4) Separating the aspirated TE cells.

provide visual feedback to the control system, aiding in the automation processes. The microscope system incorporates a motorized linear x-y stage featuring two independent stepper motors. This configuration enables the system to achieve highly accurate and precise positioning. The linear x-y stage is equipped with linear encoders with a remarkable resolution of 0.1 µm. These encoders provide precise feedback necessary for motion control in both the x-direction and the y-direction. A holding micropipette, with an outer diameter of 70 μm (Sunlight Medical Inc.), is employed in conjunction with a robotic micromanipulator (Scientifica Patchstar). The holding micropipette securely grasps the embryo using a vacuum system generating a vacuum pressure of 100 Pa. The vacuum system comprises of a pump, reservoir, and pressure regulator (Sutter Instrument). The embryo is immersed in 0.5 ml of culture media (EmbryoMax from Millipore) and carefully settled on a microscope white water glass slide measuring 2 in $\times$ 3 in $\times$ 1 mm (Premier).

The experimental system facilitates implementing and evaluating the proposed automation strategies by combining the inverted microscope, high-speed camera, and motorized linear x-y stage. The precise positioning capabilities of the stage, coupled with the imaging capabilities of the microscope and camera, contribute to the accuracy and reliability of the investigated automation processes. During the embryo rolling experiments, the microscope slide is fixed on the x-y stage. While the stage is in motion, a stationary holding micropipette applies suction to the embryo, firmly grasping it from an arbitrary location on the ZP. It is important to note that new embryos were utilized for all reported test results. This deliberate use of new embryos provides further evidence of the robustness of the computer vision algorithms, which successfully process image data and extract coordinate information from embryos with slightly varying characteristics.

IV. Embryo Reorientation

Embryo reorientation is crucial to ensure the ZP perforation is in the right location without harming the embryo's

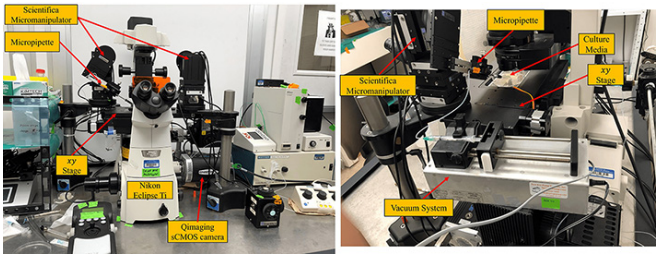

Fig. 2: The experimental setup used to verify the performance of the proposed automation method.

internal components. For human embryos, the ideal ZP perforation spot is near the ICM, while for mouse embryos, it's on the opposite side [15]. When an embryo is in contact with a stationary surface, it can be rotated in two directions by moving the contact surface. This method of reorientation, discussed in previous work [16], [17], involves sliding the embryo on the micropipette tip by moving the contact surface along different axes. This approach is being explored as an automated solution for embryo reorientation and is detailed in [16], [17].

We have developed a vision-based closed-loop control system to manage the rotation of embryos. Figure 3 illustrates the structure of the closed-loop control system with a computer vision algorithm. To explain the rotation along the x-axis, our previous work [16] revealed that the substrate moves along the y-axis, and the reverse is true for rotation along the y-axis. Initially, we control the x-y stage using a sophisticated universal microscope motion controller, enabling it to achieve highly accurate and precise tracking for a desired velocity in either the x-direction or y-direction independently. The x-y stage can be described as a first-order system for motion in the x-direction or y-direction. It takes the desired velocity as input and outputs the measured velocity. Mathematically, it can be described as

$$\frac{\dot{X}(s)}{\dot{X}_d(s)} = \frac{K_x}{\tau_x s + 1}, \quad \frac{\dot{Y}}{\dot{Y}_d(s)} = \frac{K_y}{\tau_y s + 1}, \tag{1}$$

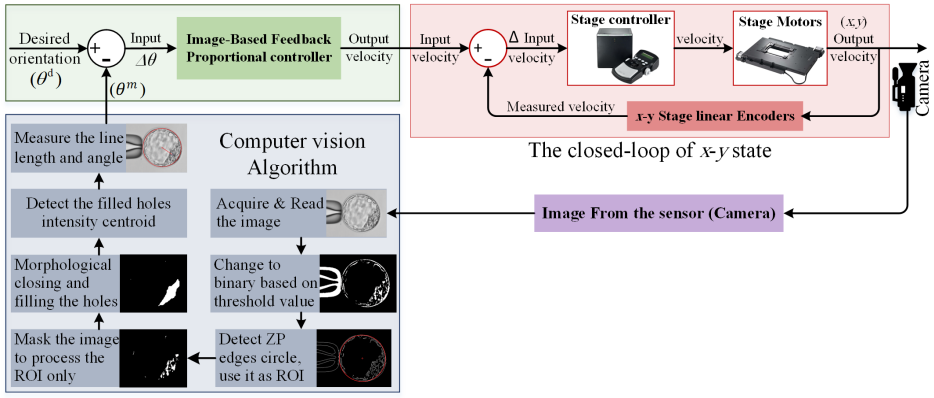

Fig. 3: The control system schematic, including the computer vision of the embryo reorientation algorithm.

where $\dot{X}_d$ and $\dot{Y}_d$ are the desired velocity of the stage applied to the controller, $\dot{X}$ and $\dot{Y}$ are the measured velocity of the stage, K_x and K_y are gain constants, τ_x, and τ_y are the time constants.

Given that the velocity of the x-y stage is regulated by a motion controller, the current control objective is to attain the desired motions in both the x-direction and y-direction. This involves ensuring that the orientation angle of the embryo, denoted as $\theta^m(t)$, tracks a desired orientation angle $\theta^d(t)$ with minimum error. As described in Figure 3, the computer vision algorithm estimates the embryo's orientation angle (θ^m). According to [17], the linear displacement c of the embryo center point and the rotation angle can be expressed by $c = r\theta_i^m$, where c can be either the x- or y-direction, r is the embryo radius, i refers to rotates about either the x- or y-axis.

The rotation control about the x-axis is independent of the rotation control about the y-axis. The following analysis is considered for the linear motion x-direction ($c = x$) and the rotation about y-axis ($i = y$). The closed-loop system with a proportional controller with a gain of K_p is given as $E_\theta(s) = \Theta^d(s) - \Theta_y^m(s)$. The error $E_\theta(s)$ can be expressed as:

$$E_\theta(s) = \frac{1}{1 + \frac{K_p K_x}{rs(\tau_x s+1)}}\Theta^d(s) \tag{2}$$

For a constant desired rotation angle with an amplitude of Θ^d, the steady-state error is given by

$$e_{ss} = \lim_{s\to 0} sE_\theta(s) = \lim_{s\to 0} s\left[\frac{1}{1 + \frac{K_p K_x}{rs(\tau_x s+1)}}.\frac{\Theta^d}{s}\right] = 0. \tag{3}$$

It can be noticed that the steady-state error for a constant desired rotation angle will always be zero. Thus, the gain K_p of the controller can be selected to achieve the desired transient performance. The transfer function of the closed loop is expressed by

$$\frac{\Theta_y^m(s)}{\Theta^d(s)} = \frac{1}{r}.\frac{K_p K_x/\tau_x}{s^2 + s/\tau_x + K_p K_x/\tau_x}. \tag{4}$$

Since the dynamic system exhibits inherent stability, the value of K_p is determined through experimentation. The experimental results demonstrate that gain values within a range of $0.5 \leq K_p \leq 1$ yield satisfactory dynamic behavior with consistent repeatability. Figure 4 provides an illustrative example of these experiments.

In Figures 4(a)-(c), the substrate undergoes motion in the x-direction (indicated by the red arrows) to facilitate embryo rotation about the y-axis. Conversely, in Figure 4(d), the substrate moves in the y-direction (as denoted by the green arrow) to achieve embryo rotation around the x-axis. Figure 4(e) demonstrates that the algorithm halts substrate motion when θ^m and the line length fall within the desired ranges. Estimations of embryo orientation are based on the ICM location, and the motion and rotation axes are clearly indicated in each frame. The scale bar measures 25 μm.

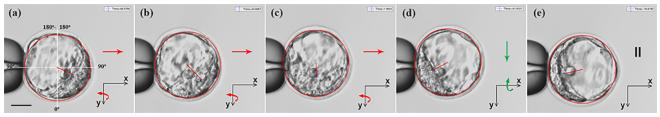

Fig. 4: Experimental results of the Embryo reorientation experiment. The scale bar in (a) is 25 μm.

V. Zona Pellucida Perforation Automation

After successfully orienting the embryo, the next step involves making a hole in its outer membrane, known as the ZP. This hole allows access to the embryo's inside, where a few TE cells can be extracted for analysis using a biopsy micropipette. To achieve precise perforation of the ZP, a laser perforation method can be used, which creates a longitudinal trench similar to the natural rupture of the ZP during natural hatching. Automating the laser perforation process can improve its success rate and ensure the embryo's safety. Figure 5 shows a schematic diagram of the vision-based feedback control system for relocating the embryo.

A. Perforation algorithm

The proposed method for automating the perforation of the ZP is shown in Figure 6. This process involves several key steps to achieve accurate and precise perforation while maintaining the desired orientation of the embryo. First, the embryo is securely held in place with increased suction applied to the micropipette (typically around 700 Pa), as determined through experiments (see Figure 6(a)). Next, an

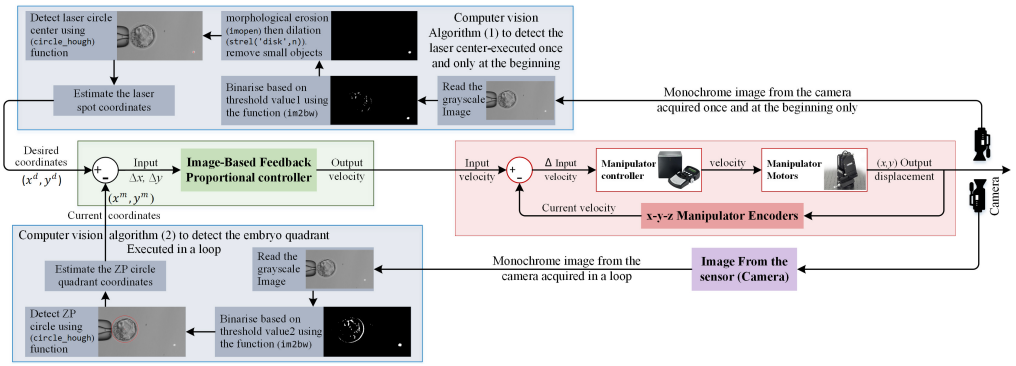

Fig. 5: The schematic diagram of the vision-based feedback control system used to relocate the PL toward the laser spot. The blue containers are the computer vision algorithms that estimate (x_1, y_1) and (x_2, y_2).

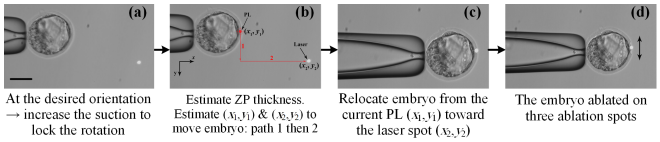

Fig. 6: The ZP perforation algorithm steps motion from (a) through (b) to get to the desired location shown in (c) and perforate the ZP as shown in (d). The scale bar is 25 μm.

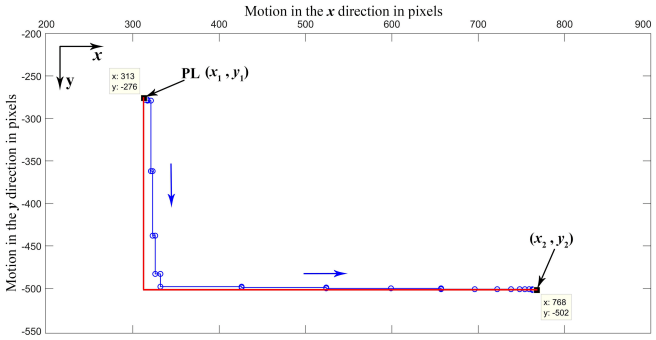

Fig. 7: The control system response for relocating the PL position from (x_1, y_1) towards (x_2, y_2). Red is the desired path, and blue is the real motion path. The arrows refer to the motion direction.

algorithm determines the perforation position relative to the laser spot and estimates the ZP thickness. Based on this information, laser parameters like pulse duration, number of pulses, and pulse power are adjusted to ensure effective ZP ablation (see Figure 6(b)). To perform the ZP ablation, the embryo is precisely repositioned under the microscope using vision-based feedback control. The micropipette is maneuvered to align the embryo's ZP perforation position with the fixed coordinates where the laser will create the initial trench (as shown in Figure 6(c)). Then, the embryo is moved along the $\pm y$ direction, parallel to the y-axis, to ablate two more trenches (see Figure 6(d)). After the ablation process, the embryo remains in place, ready for the subsequent extraction of TE cells.

B. Relocating the embryo

The robotic micromanipulator, equipped with a micropipette, is directed to transport the embryo from the coordinates (x_1, y_1) of the perforation point (PL) to the laser spot's designated location (x_2, y_2), as illustrated in paths 1 and 2 within Figure 6(b). This micromanipulator is equipped with *xyz*-linear stages, granting individual control over each axis through an automated motion controller. The control system for relocating the embryo establishes the perforation position (PL) concerning the laser spot. This calculation follows an estimation of the outer and inner circles of the ZP, with PL positioned precisely at the midpoint between the quadrants of these two circles. The desired position (x^d, y^d) corresponds to the coordinates of the laser spot, denoted as (x_2, y_2), primarily determined using a computer vision algorithm (1). Concurrently, the current location of PL, represented as (x^m, y^m), is estimated in real-time through another computer vision algorithm (2), providing vital vision-based feedback for the control system. The camera initially captures the image presented in Figure 6(a) with a brief exposure time of 5μs. Two computer vision algorithms, outlined in Figure 5, extract the coordinates of PL (x_1, y_1) and the coordinates of the laser spot location (x_2, y_2), which are then fed into a proportional controller. The discrepancy between these two coordinate sets signifies the spatial separation between the two locations. This camera continues to acquire images in each iteration of the control loop. Two proportional controllers with a gain K_{px} and K_{py} are used to achieve the desired coordinates (x^d, y^d). Figure 7 shows a typical control system response.

C. Determination of the laser parameters

The ZP perforation algorithm estimates ZP thickness by initially identifying its outer and inner circles through a computer vision algorithm (2), as depicted in Figure 5. The algorithm calculates ZP thickness by measuring these circle diameters. Subsequently, the perforation algorithm adjusts laser power intensity and pulse duration based on this thickness value. In this research, we maintained the power intensity at the maximum laser system value (300 mW) to minimize energy transfer to the embryo. Conversely, we tailored the pulse duration, ranging from 400 to 500 μs, based on ZP thickness. This simplifies parameter adjustment by fixing one parameter (power intensity) while modifying

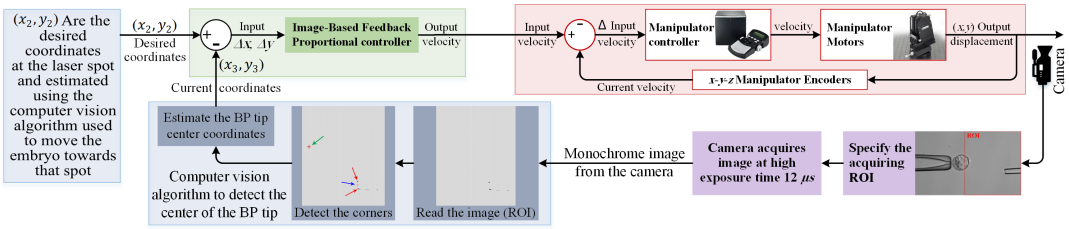

Fig. 8: The control system used to move the Biopsy micro Pipette tip center (BP) towards the protruded TE cells position (PL). Red arrows refer to the BP corners, blue refers to its tip center, and green refers to the laser spot.

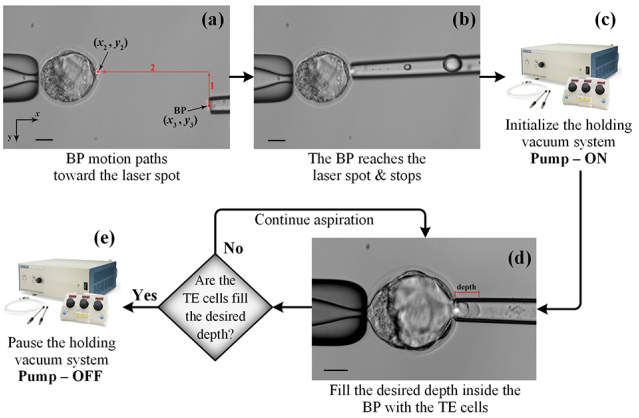

Fig. 9: Aspiration algorithm steps. In (a) and (b), the BP relocated toward the perforated position. From (c) to (e), the TE cells fill the desired depth in BP. The scale bar is 25 μm.

the other (pulse duration). This approach aimed to optimize laser parameters for ZP perforation, considering the specific characteristics and needs of the embryos under study. The ZP was ablated at three locations: one at the position shown in Figure 6(c), and two at predetermined positions in the $\pm y$-direction from the initial ablation, as seen in Figure 6(d), and since the motion is along the vertical axis only, then an open-loop controller moved the embryo to these second and third ablation sites. This displacement corresponded to ± 0.9 of the ZP thickness, determined through experimentation. The initial perforation opens the ZP, while subsequent ablations weaken the ZP around the initial site. This allows the ZP to stretch, enabling the biopsy pipette to extract TE cells while keeping other embryo components within the ZP.

VI. TE Cells Extraction Automation

After the embryo's ZP is perforated, the TE cell layer naturally starts to emerge through the perforation, allowing the aspiration of multiple TE cells without disrupting the TE layer's structure. Extracting TE cells is a pivotal phase in the biopsy process as it entails ablating and isolating these protruding TE cells. Mishandling this process may result in the complete hatching of the embryo, which could severely impact its development or even lead to its demise.

A. Trophectoderm cells aspiration algorithm

Under vision-guided closed-loop control, a biopsy micropipette is positioned to make contact with the tip of the TE cells emerging from the previously perforated ZP. These TE cells are then aspirated, causing them to stretch in a direction perpendicular to the ZP perforation and away from it. This preparation sets the stage for a multi-pulse laser to ablate the TE cell-to-cell connections of these stretched TE cells, making it possible to biopsy the cells held within the biopsy micropipette. The entire process is meticulously managed using a vision-based control system. During the aspiration process, a holding micropipette keeps the embryo steady, while a biopsy micropipette featuring an inner diameter of 20 μm and connected to a microliter syringe pump generates suction. This suction draws the protruding TE cells from the ZP perforation into the biopsy micropipette. The length of the aspirated TE cells within the biopsy micropipette is visually monitored, allowing for precise control over the pump's vacuum to aspirate the desired number of TE cells.

B. Relocating the biopsy micropipette

The biopsy micropipette is moved to the desired aspiration position through a vision-based feedback control system, as depicted in Figure 8. The camera initially captures an image, as shown in Figure 9(a), using a 15 μs exposure time. In the schematic in Figure 8, a computer vision algorithm is employed to estimate the coordinates (x_3, y_3) of the center of the BP, while the desired coordinates (x_2, y_2) for the ZP perforation position are predetermined and known from the previous ZP perforation step. Both coordinates are then used as inputs for a proportional controller within the algorithm.

The proportional controller calculates the difference between the current and desired positions of the biopsy micropipette, aiming to minimize this distance. The camera consistently captures images in each control loop, providing ongoing feedback. The control loop iterates until the coordinates' difference reaches zero or falls within the desired range. Figure 9(a) visually displays the positions of the BP and the laser spot, offering a clear representation of their locations. Furthermore, Figure 10 demonstrates the control system's response during the relocation of the biopsy micropipette. The intended motion path is shown in grey, while the actual motion path is depicted in red.

C. Tracking the TE cells inside the biopsy micropette

Once the BP aligns with the perforation location (PL), the control algorithm activates the syringe pump in withdrawal mode to initiate TE cell aspiration. This process is regulated by estimating the number of TE cells aspirated, filling a

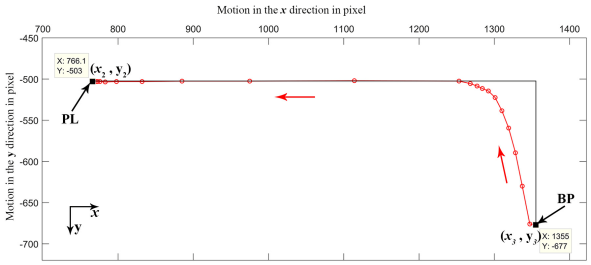

Fig. 10: The response of the control system used for relocating the BP position from (x_3, y_3) toward the PL position (x_2, y_2). The grey line is the desired path. The red line is the real path. The red arrows refer to the motion direction.

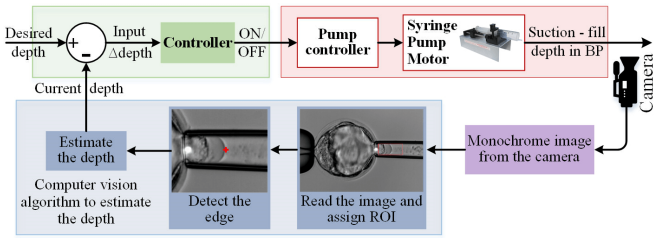

Fig. 11: The vision-based control system used to control the aspiration pump according to the tracking algorithm shown in the blue container.

predefined volume determined to be over 15μm inside the biopsy micropipette. Visual monitoring is used to track the length of TE cells aspirated into the BP, thereby controlling the vacuum pump. Figure 11 provides a schematic of the vision-based control system for tracking TE cells within the biopsy micropipette. Multiple experiments involving the relocation of the biopsy micropipette, TE cell aspiration, and tracking were performed to assess the control system's effectiveness. Figure 9 presents one such experiment.

VII. Separating the Aspirated TE Cells

A. TE cells ablation for separation algorithm

The separation process of the TE cells begins once they have reached a predetermined depth inside the biopsy micropipette. The computer vision tracking algorithm (Figure 9) signals the ablation control algorithm to deactivate the vacuum pump and initiate the TE cell separation through ablation. This separation is facilitated by the algorithm outlined in Figure 12. During ablation, a low-power intensity laser with a short pulse duration selectively removes cell-to-cell connections among the stretched TE cells outside the aspiration micropipette. This combination ensures precise and efficient ablation, separating the aspirated TE cells. The automation system accurately detects the conditions necessary to initiate the ablation process using computer vision tracking and appropriate laser parameters, guaranteeing effective TE cell separation during the biopsy procedure.

The process involves stretching the cell-cell connections and increasing the laser pulse rate to initiate the ablation step. This stretching is achieved by moving the biopsy micropipette away from the stationary embryo while it holds the aspirated TE cells. Experimentally, it was found that

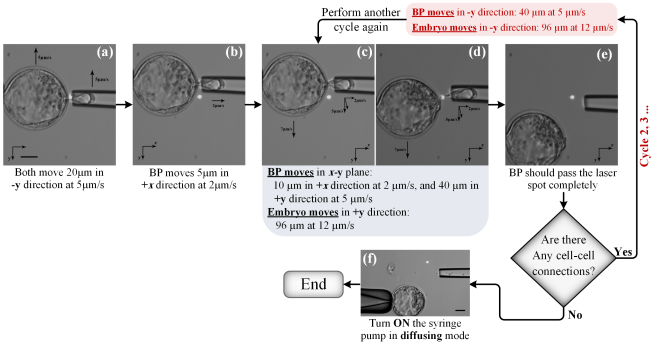

Fig. 12: TE cells separation algorithm. The bar is 25 μm.

more stretching of the connections leads to better ablation results. Therefore, the algorithm continues to stretch the connections during laser ablation by moving the biopsy micropipette away from the embryo. Both the embryo and the biopsy micropipette move in the $+y$-direction but at different velocities. This differential motion further stretches the connections and simultaneously prevents the aspirated TE cells from exiting the biopsy micropipette.

B. Vision-guided closed-loop algorithm

This section elucidates the steps, movements, and velocities integral to the vision-guided closed-loop algorithm. The explanations below detail the motion of both the embryo and the biopsy micropipette, including their respective velocities.

1) The embryo and the biopsy micropipette are directed to move at a velocity of 5 $\mu m/s$ in the $-y$ direction, away from the laser spot, covering a distance of 20 μm. This maneuver is intended to align the cell-to-cell connections precisely over the laser spot, as illustrated in Figure 12(a).
2) The biopsy micropipette moves 5 μm at a speed of 2 $\mu m/s$ in the $+x$ direction to stretch the cell-to-cell connections, as it is illustrated in Figure 12(b).
3) To keep the stretched connections positioned above the laser spot, the biopsy micropipette performs two concurrent movements: it travels 10 μm in the $+x$ direction at a speed of 2 $\mu m/s$. It simultaneously moves 40 μm in the $+y$ direction at a velocity of 5 $\mu m/s$. In parallel, the embryo shifts 96 μm upward in the $+y$ direction at a rate of 12 $\mu m/s$. These coordinated movements are depicted in Figure 12(c) and (d).
4) Once the embryo and the biopsy micropipette are positioned together over the laser spot, as depicted in Figure 12(c) to (e), the laser initiates the ablation.
5) Upon completing the initial cycle and ablating the TE cell connections (as depicted in Figure 12(e)), the suction pump within the biopsy micropipette is employed to apply positive pressure. This positive pressure serves to disperse the TE cells and expel them from the biopsy pipette, as demonstrated in Figure 12(f).

These synchronized motions and velocities, under the guidance of the computer vision system, facilitate precise control of both the embryo and the biopsy micropipette throughout the ablation and TE cell extraction procedures.

VIII. Discussion and Conclusion

This research introduces methods for automating the TE cells aspiration and separation as an integrated step in the blastocyst embryo biopsy procedure. Leveraging readily available tools in research labs and IVF clinics, it integrates computer vision and image-based control algorithms to enhance the precision and efficiency of the biopsy procedure. Image-based control algorithms enable precise tool manipulation for ZP perforation, in preparation for the TE cells aspiration and then separation, reducing the risk of embryo damage. These techniques enable automation without needing specialized equipment, making them suitable for adoption in existing labs and clinics. The automation techniques employed closely replicate the manual techniques currently employed by highly skilled embryologists. The results obtained show a 100% success rate. Compared to the manual techniques currently being used in labs, the success rate is 34.5% to 44.3% according to [18].

The results presented in Table 1 utilized newly generated embryos that demonstrate the reliability of the computer vision algorithms in effectively processing image data and extracting coordinate information from various embryos. The high success rate observed in our experiments can be attributed to several key factors. Employing a highly rigorous experimental design, including comprehensive pre-testing and optimization phases, which allowed us to refine our methods and reduce potential error. The experiments were conducted under controlled conditions with minimal variability, allowing us to closely monitor and adjust parameters as necessary. The use of advanced vision-based technologies ensured precise and repeatable actions. The team's expertise and careful execution.

TABLE I: The experimental results. A single embryo was used for each procedure to pass through all its steps. Some extra experiments were performed for a single step only.

The step	Experimental parameters		The results
Reorientation step	Number of Experiments.		12
	Closed loop update rate in Hz.		4.1
	Starting angle (degree).	Refer to Figure 4 for angles distribution	Random
	Last angle (degree).		-76.8 to -102.4
	Desired angle (degree).		-70 to -110
	Success rate: Rotate the embryo to the desired range.		100%
Embryo relocation and ZP ablation steps	Number of experiments.		16
	Closed loop update rate (embryo relocation) Hz		3.4
	Closed loop update rate (ablation and its motion) Hz.		3.3
	Laser exposure time (μs).		$400 - 450$
	Success rate: PL relocated to be at BP and 3 spots ablated		100%
TE Cells Tracking	Number of experiments.		9
	Cycle time (s).		$20 - 25$
	Success rate: Detect the TE cells and pause the pump.		100%
TE Cells Separation	Number of experiments - single attempt.		8
	Number of experiments - two attempt.		1
	Cycle time (s) - without the diffusing time.		18
	Laser pulse duration time (μs).		200
	Number of laser pulses in second (pulse/s)		$1.75 - 2$
	Success rate: Complete the separation motions. Separate the aspirated TE cells.		100%

Human and Animal Research Disclosure Approval

All experiments were performed on mouse embryos at the blastocyst stage obtained by means approved by the University of Toronto Health Sciences Research Ethics Board and the Local Animal Care Committee. All experiments were approved by the Animal Care and Use Committee of the University of Toronto.

Acknowledgment

The authors wish to acknowledge the contribution of the Center of Phenogenomics (TCP), Toronto, Canada for providing the embryos used in the experiments.

References

[1] M. N. Moufarrej and S. R. Quake, "An inexpensive semi-automated sample processing pipeline for cell-free rna extraction," *Nature Protocols*, pp. 1–22, 2023.

[2] M. Alexovič, J. Sabo, and R. Longuespée, "Automation of single-cell proteomic sample preparation," *Proteomics*, vol. 21, no. 23-24, p. 2100198, 2021.

[3] I. Dimitriadis, N. Zaninovic, A. C. Badiola, and C. L. Bormann, "Artificial intelligence in the embryology laboratory: a review," *Reproductive biomedicine online*, vol. 44, no. 3, pp. 435–448, 2022.

[4] G. Shan, Z. Zhang, C. Dai, H. Liu, X. Wang, W. Dou, and Y. Sun, "Robotic cell manipulation for blastocyst biopsy," in *2022 International Conference on Robotics and Automation (ICRA)*. IEEE, 2022, pp. 7923–7929.

[5] J. J. Berger, "Primum non nocere: are we closer to saying that the trophectoderm biopsy does no harm?" *Fertility and Sterility*, vol. 112, no. 1, pp. 35–36, 2019.

[6] G. Shan, C. Dai, H. Liu, X. Wang, W. Dou, C. Ru, Z. Zhang, and Y. Sun, "Robotic blastocyst biopsy," *IEEE/ASME Transactions on Mechatronics*, vol. 28, no. 3, pp. 1372–1383, 2023.

[7] V. Raudonis, A. Paulauskaite-Taraseviciene, K. Sutiene, and D. Jonaitis, "Towards the automation of early-stage human embryo development detection," *Biomedical engineering online*, vol. 18, no. 1, p. 120, 2019.

[8] E. P. Consortium, S.-E. B. W. Group, G. Kokkali, G. Coticchio, F. Bronet, C. Celebi, D. Cimadomo, V. Goossens, J. Liss, S. Nunes, I. Sfontouris *et al.*, "ESHRE PGT consortium and SIG embryology good practice recommendations for polar body and embryo biopsy for PGT," *Human reproduction open*, vol. 2020, no. 3, pp. 1–12, 2020.

[9] E. Casser, S. Israel, A. Witten, K. Schulte, S. Schlatt, V. Nordhoff, and M. Boiani, "Totipotency segregates between the sister blastomeres of two-cell stage mouse embryos," *Scientific reports*, vol. 7, no. 1, p. 8299, 2017.

[10] Y. Mizobe, Y. Kuwatsuru, Y. Kuroki, Y. Fukumoto, M. Tokudome, H. Moewaki, M. Watanabe, T. Iwakawa, and K. Takeuchi, "A novel trophectoderm biopsy technique for all blastocyst stages," *Reproductive Medicine and Biology*, vol. 21, no. 1, pp. 1–7, 2022.

[11] K. Rao, *Principles & Practice of Assisted Reproductive Technology (3 Vols)*. JP Medical Ltd, 2013, vol. 1.

[12] B. A. Zanouneh and J. K. Mills, "Cell extraction automation in single cell surgery using the aspiration method," in *2022 International Conference on Manipulation, Automation and Robotics at Small Scales (MARSS)*. IEEE, 2022, pp. 1–6.

[13] Y. Zhang, X. Li, S. Gao, Y. Liao, Y. Luo, M. Liu, Y. Bian, H. Xiong, Y. Yue, and A. He, "Genetic reporter for live tracing fluid flow forces during cell fate segregation in mouse blastocyst development," *Cell Stem Cell*, vol. 30, no. 8, pp. 1110–1123, 2023.

[14] C. Y. Wong and J. K. Mills, "Cell extraction automation in single cell surgery using the displacement method," *Biomedical microdevices*, vol. 21, pp. 1–11, 2019.

[15] D. K. Gardner, A. Weissman, C. M. Howles, and Z. Shoham, *Textbook of assisted reproductive techniques fourth edition: volume 2: Clinical perspectives*. CRC press, 2012, vol. 2.

[16] I. A. Ajamieh, B. Benhabib, and J. K. Mills, "Automated system for cell manipulation and rotation," in *2018 IEEE International Conference on Mechatronics and Automation (ICMA)*. IEEE, 2018, pp. 2334–2339.

[17] I. Abu Ajamieh, B. Benhabib, and J. K. Mills, "Automatic system for the blastocyst embryo manipulation and rotation," *Annals of biomedical engineering*, vol. 48, pp. 426–436, 2020.

[18] E. J. Yu, E.-A. Park, S.-A. Choe, K.-A. Lee, and Y. S. Kim, "Freeze all-first versus biopsy-first: A retrospective analysis of frozen blastocyst transfer cycles with preimplantation genetic testing for aneuploidy," *PLOS ONE*, vol. 17, pp. 1–10, 2022.